Physica B 673 (2024) 415490

Contents lists available at ScienceDirect

Physica B: Condensed Matter

journal homepage: www.elsevier.com/locate/physb

Enhancement of lithiation on a graphane monolayer through extended H vacancy pathways: An ab initio study

S.P. Kgalema [a,1], M. Diale [a,1], E. Igumbor [b,1], R.E. Mapasha [a,1,*]

[a] Department of Physics, University of Pretoria, Hatfield campus, Pretoria 0002, South Africa
[b] Department of Mechanical Engineering Science, University of Johannesburg, Johannesburg, South Africa

ARTICLE INFO

Keywords:
Density functional theory
Graphane
Hydrogen vacancies
Li-ions batteries
Lithiation potential
Storage capacity

ABSTRACT

The increasing interest for the need of large-scale energy-storage systems have led to the development of high-performance energy-storage devices such as lithium-ion batteries (LIBs). Two dimensional (2D) materials are promising candidates for fulfilling this requirement due to their peculiar physical properties. However, it is important to understand the role of multiple Li adatoms on the 2D materials, more especially when defects are involved. In this study, first-principles density functional theory (DFT) calculations were performed to study Li on the H vacancies (V_H) following the line and zigzag pathways on a graphane sheet. The results of Li atom on a single H vacancy (V_{H1}) reveal an immediate enhanced interaction based on the improved binding energies, high amount of charge transfer and significantly shortened Li height, as compared to those of pristine graphane counterpart. An increase in the number of H vacancies along the line pathway from one (V_{H1}(L)) to five (V_{H5}(L)) further improves the binding energies ranging from 1.82 eV to 2.91 eV. Considering a simultaneous increase of Li atoms and H vacancies following a line pathway (V_{H1}(L) to five V_{H5}(L)), the binding energies tend to reduce in order. However, it is still higher than the minimum Li standard bulk cohesive energy of 1.63 eV. We show that there is a possibility of uniform dispersion of Li atoms with less clustering on a graphane sheet. A transition from insulator to metallic character was observed from V_{H1}(L) to V_{H5}(L), due to an induced new Li states at the vicinity of the Fermi level, suggesting an enhancement of electronic conductivity in the graphane sheet. At five Li atom V_{H5}(L) configuration along the line pathway, we obtained a relatively high storage capacity of 207.49 mAh/g with its corresponding lithiation potential of 1.48 V, comparable to those of well known two dimensional anode materials.

1. Introduction

The global energy interest is rapidly shifting away from the well-known fossil fuel cell to the renewable energy sources, such as solar cells, wind energy, and geothermal energy [1–3]. However, the power generation from these well known energy sources does not meet the current global energy demand [4]. Consequently, the development of large-scale energy-storage systems that can address this energy disparity is required. Significant efforts by both theoretical and experimental researchers have been made towards developing high-performance energy-storage devices such as lithium-ion batteries (LIBs) [5,6] and supercapacitors [7,8]. Over the past two decades, LIBs have been widely used as a power source for electronic device operations [5,6,9].

Graphite is the most commonly used anode material for LIBs due to its ability to reverse Li ions intercalation, abundance in nature and less toxicity [10]. The graphite's theoretical maximum lithium storage capacity of 372 mAh/g at around 700 degrees Celsius [11] is too small to fulfil the current global energy demand. The recent miniaturization of electronic device sizes also poses a great challenge to graphite in terms of device fabrication. More research efforts have been redirected towards finding the anode materials with dramatic performance requirements, such as high volumetric energy density, rapid cyclability, fast charging rate, high stability and less toxicity [12]. The aforementioned properties can collectively be achieved through consideration of a special material. Concerted efforts have been directed towards the two dimensional (2D) materials as a new avenue of replacing stacked layered graphite in LIBs.

Graphene and its derivative (graphane) emerged as promising candidates for anode in LIBS, owing to their large contact area (a property required for specific capacity) and stability at room temperature [13–18]. Both the experimental and theoretical studies reported that graphene can be used as anode material in LIBS due to its high thermal and electrical conductivities, large surface area (possibility

* Corresponding author.
E-mail address: Edwin.mapasha@up.ac.za (R.E. Mapasha).
[1] Contributed equally to the writing of this manuscript.

https://doi.org/10.1016/j.physb.2023.415490
Received 23 May 2023; Received in revised form 9 October 2023; Accepted 6 November 2023
Available online 8 November 2023

of accommodating Li atoms on both sides of the sheet) and high mechanical strength [14–17,19,20]. Previous study by Chan et al. [21] indicated that Li binding energy depends on the adsorption site. The hollow, bridge and top sites have the binding energies of 1.10 eV, 0.77 eV and 0.75 eV, respectively [21]. The bonding nature between Li and graphene is ionic with a significant amount of charge transfer. The aforementioned binding energies are smaller than the standard bulk cohesive energy of 1.63 eV, understandably this would lead to the formation of the undesired Li clustering above the graphene sheet [22–26]. Although, there are several methods to improve the reactivity graphene such as doping, some researchers shifted their focus to other 2D materials such as graphane as potential electrode materials for LIBs.

Graphane has lately received significant research attention owing to its semiconducting characters and low dimensionality, the excellent properties required by recent miniaturized electronic devices. Graphane was first predicted by the theoretical methods [27,28] and later validated through various experimental techniques [18]. The latter revealed that under hydrogen plasma, graphane can be achieved at around 24 °C (excellent condition for most electronic devices operation) and the dehydrogenation starts to take place at around 450 °C through annealing in argon. Graphane have different isomers, namely the stirrup, boat and chair configurations [29]. It was revealed theoretically that the latter configuration is most stable, which was supported through experimental characterizations [18]. Due to high surface area and low dimensionality of chair graphane [29], it can be used as anode material in future LIBs. However, this will be difficult to achieve due to its inertness while reacting with Li atoms. Yang et al. [30] reported that the H atoms on the graphane layer screens the external charges offered by Li atoms. Watcharinyanon et al. experimentally reported the existence of Li islands on a graphane monolayer which disappear after annealing, leading to the formation of LiH dimers [31].

The improvement of Li–graphane interaction could enhance its application as 2D anode material. The simplest technique one can think of is the surface modification giving rise to the reactive sites. Creation of vacancies is a renowned possibility of graphane surface modification. For instance, the removal of hydrogen (V_H) and carbon with hydrogen as pair (V_{CH}) [29,32–34]. Various computational studies revealed that the formation of V_H is endothermic [29,33]. Also, experimental study reports that vacancies can be created by continuous exposure of high energy electron beam or irradiation with low-energy Ar^+ [35]. The single V_H causes the localized states at the vicinity of Fermi level, with a magnetic moment of $1\mu_B$ due to the dangling bond. This is an indicative that graphane with V_H can positively react with foreign atoms. Previous theoretical studies report that Li replacing H atom has a higher binding energy than the Li bulk's cohesive energy reducing the chances of cluster formations. It was further concluded that the Li doped graphane is suitable for H_2 storage based on the improved hydrogen storage capacity and adsorption energies [36,37]. The information of multiple Li adatoms on the V_H vacancies is still missing, more especially on the electrochemical properties for LIBs.

In this work, using DFT method we investigate the energetic stability, electronic properties and electrochemical properties of the multiple Li adatoms on the V_H vacancies in a graphane monolayer following the line and zigzag pathways. Our calculated lithiation voltages and storage capacities are compared with those of graphene and other 2D materials. Our results encourages the experimental characterization of graphane monolayer with V_H vacancies to assess their viability at various conditions.

2. Methodology

In this study, the electronic structure calculations were performed using DFT approach [38,39] with a projected augmented wave (PAW) pseudopotential method [40] for the nucleus and electron interaction description. We employed the Vienna ab initio simulation package (VASP) [41] for all calculations. The exchange correlation energy part was described using the Perdew–Burke–Ernzerhof variant of the generalized gradient approximation (GGA-PBE) [42]. The accuracy of the DFT simulation depends on the various input parameters used to compute the properties of the material system. To obtain the accurate results, the tests of total energy convergence for the energy cut-off, the number of k-points and supercell sizes were carried out. An energy cut-off of 400 eV for the expansion of the plane waves is sufficient and a Monkhorst Pack [43] k-meshes of $4 \times 4 \times 1$ ($12 \times 12 \times 1$) is suitable for generating k-points that can adequately sample the Brilloiun zone during electronic structural relaxations (densities of states calculations). The high cut-off energy of 1800 eV for the augmentation of the electronic charge was set in the incar file. A converged $5 \times 5 \times 1$ supercell consisting of 50 C and 50 H atoms was used for all calculations. The total energies criteria were set at a difference of less than 1×10^{-4} eV, and for the force convergence it was set to differences of less than 1×10^{-3} eV/Å. This study takes into account the supercell periodic boundary conditions, and the interlayer spacing along the z-axis was set to 10 Å in order to avoid spurious periodic image interactions.

3. Results and discussion

Understanding the binding of adatoms on the substrate is an important aspect for application of electrode material in a LiBs. In this section, different Li adsorption sites were identified on a converged $5 \times 5 \times 1$ supercell of a graphane sheet with or without a H vacancy (V_H) as depicted in Figs. 1. The most stable site based on the geometry optimization calculations was established. Figs. 1(a) and (b) each presents four distinct Li adsorption sites on a pristine graphane sheet and on graphane with a V_H hydrogen vacancy. From Fig. 1(a), b_{site}, h_{site}, H_{site} and C_{site} represent where the adsorption of Li occurs between the two nearest neighbour C atoms (bridge site), on a centre of hexagon, on top of H atom and on top of C atom sites, respectively. Furthermore, Fig. 1(b) presents graphane sheet with a V_H. In the above mentioned case, the unique Li adsorption sites only considered at the vicinity of V_H are b'_{site}, h'_{site}, $V_{H\,site}$ and C'_{site}. The above scenario shows the adsorption of Li between V_H and its nearest neighbour C atom (bridge site), on a centre of hexagon, on top of C atom with V_H and on top of C atom neighbouring V_H site as shown in Fig. 1(b), respectively.

Furthermore, we investigated the mediation of the multiple H vacancies (V_H) on the energetic stabilities of Li on graphane. The multiple H vacancies were created following different arrangements; random (R) configuration, line (L) and zigzag (Z) pathways on graphane as shown in Figs. 2(a), (b) and (c). Typically, a random configuration is created by randomly removing the H atoms on both sides of graphane sheet. V_{H1}(R), V_{H2}(R), V_{H3}(R), V_{H4}(R) and V_{H5}(R) refer to one, two, three, four and five H vacancy configurations in a random disordered Fig. 2(a). A line V_H configuration was systematically created by removing the H atoms on one side of the sheet along a line in a continuous manner as shown in Fig. 2(b). V_{H1}(L), V_{H2}(L), V_{H3}(L), V_{H4}(L) and V_{H5}(L) refer to one, two, three, four and five H vacancy configurations along the line pathway. For the zigzag V_H configurations, the H atoms were removed on both sides of the graphane sheet in an alternating manner indicating a chain pattern shown in Figs. 2(c). For example, the V_{H2}(Z) and V_{H10}(Z) indicates the two and ten vacancies following the zigzag pathway.

As a norm, it would be therefore meaningful to compare the energies of three configurations and establish the most preferred configurations. Once the preferred configurations are identified, then the process of lithiation can take place. In this work, configurations with the same number of vacancies are compared, based on the following calculated formation energy expression (1).

$$E_f(V_H) = E_{tot}(V_H) - E_{tot}(G) + \sum n_H \mu_H. \quad (1)$$

$E_{tot}(V_H)$ is the total energy of V_H configuration and $E_{tot}(G)$ is that of graphane. μ_H is considered to be chemical potential of H referenced to the total energy of hydrogen molecule and n_H is the number of H

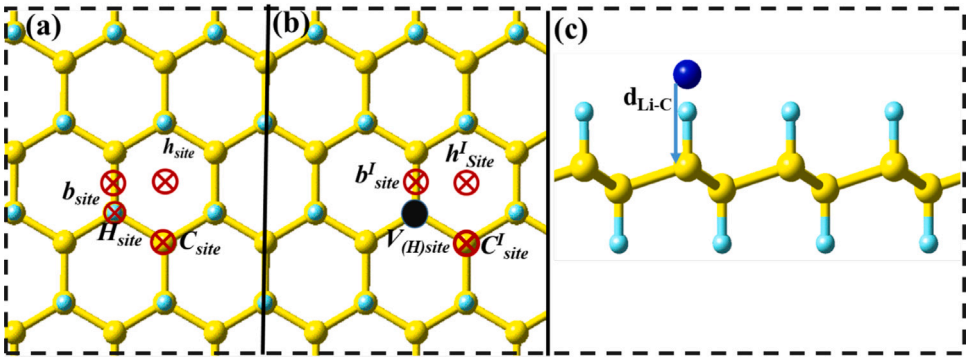

Fig. 1. The top views of an unrelaxed (a) pristine graphane sheet and (b) graphane with a V_H vacancy, respectively. (c) The side view of a graphane sheet with Li atom. Light blue, yellow and dark blue spheres represent H, C and Li atoms. Red crossed circles indicate the possible Li adsorption sites and the black dot represents V_H. The acronyms b_{site}, h_{site}, H_{site} and C_{site} represent the possible Li adsorption sites on a pristine graphane, while b'_{site}, h'_{site}, $V_{H\,site}$ and C'_{site} represent those sites near a V_H vacancy. d_{Li-C} denotes bond distance between Li and C, respectively.

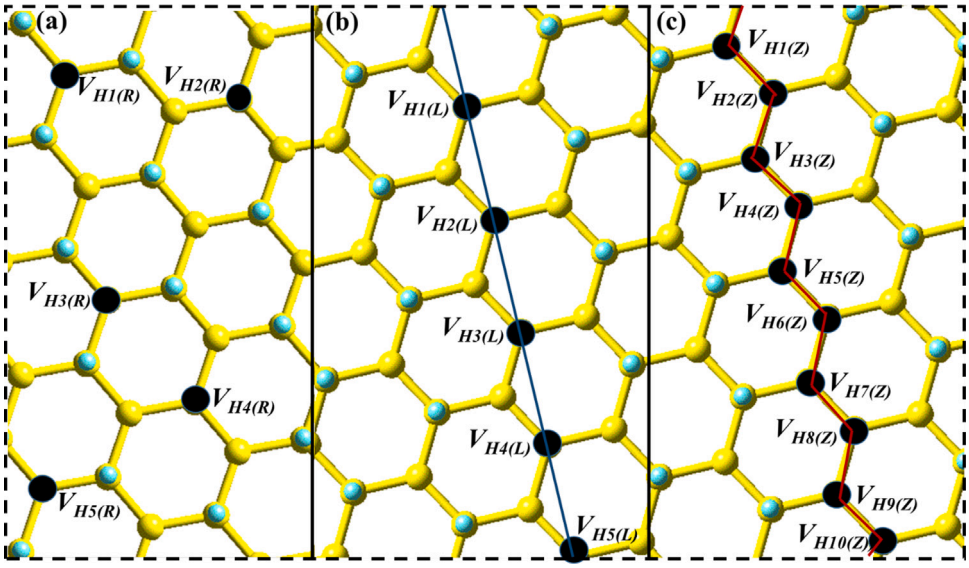

Fig. 2. The unrelaxed structures showing the multiple H vacancy sites. (a) H vacancies in a random (R) configuration (b) H vacancies along the Line (V_H(L)) pathway and (c) H vacancies along the zigzag (V_H(Z)) pathway. The blue and red lines indicate the line and zigzag pathways, respectively.

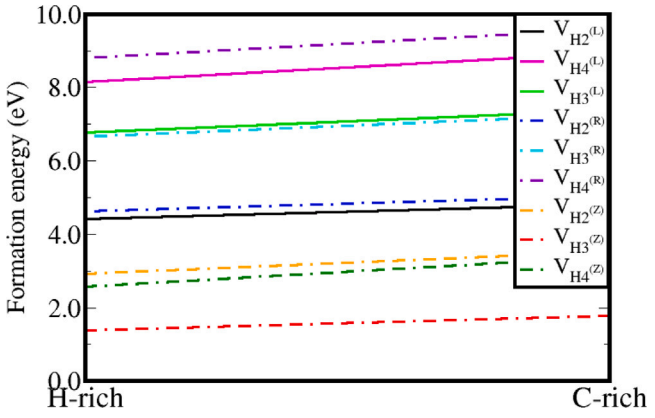

Fig. 3. The calculated formation energies of different H vacancies configurations: random (V_H(R)), Line (V_H(L)) and zigzag (V_H(Z)) with respect to the number of vacancies. The formation energies is calculated with respect to change in H chemical potential considering up to extreme conditions (H-rich and C-rich).

vacancies created. Furthermore, we allowed the formation energies of the V_H configuration to vary with respect to H chemical potential μ_H and C chemical potential μ_C (Fig. 3), representing growth conditions. The growth conditions may vary from C-rich (μ_H is low) to H-rich (μ_H is high). The possible values of μ_H and μ_C have to be obtained obeying those conditions. For a complete graphane (CH), the thermodynamic equilibrium μ_H and μ_C should satisfy the following:

$$\mu_C + \mu_H = \mu_{CH} \tag{2}$$

Under H-rich condition, μ_H is the energy obtained from half hydrogen molecule and its corresponding μ_C (dependent chemical potential) is obtained from (2). Under C-rich, μ_C is deduced from the total energy of graphene monolayer, while its corresponding μ_H is obtained from (2).

All the random (R), line (L) and zigzag (Z) configurations have positive formation energies (endothermic reaction), and this is typical for vacancy defects into two dimensional materials [29]. The possibility of endothermic reaction is constantly noted in both extreme conditions as shown in Fig. 3. Furthermore, increasing the number of H vacancies (two to four) raises the formation energy of each configuration. Fig. 3 also shows that the zigzag (Z) configuration has lowest energy, while line (L) and random (R) are competing in stability. Creating a V_H in graphane, the carbon atom in which the missing H was bonded to return to the Graphene-like configuration with localized electron (dangling bond) leading to partially filled state at the Fermi level.

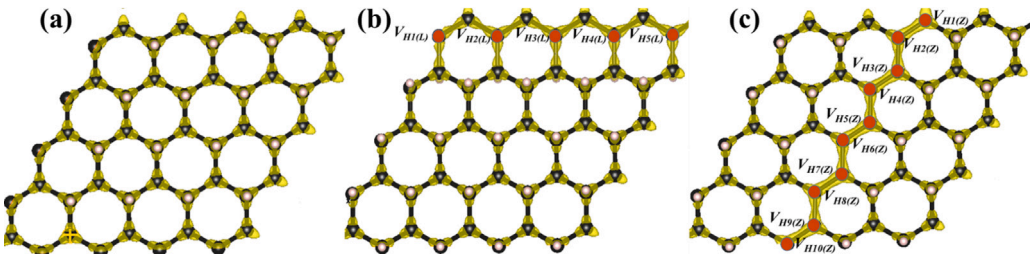

Fig. 4. The electronic charge density distribution for the (a) pristine graphane, (b) Line (L) and (b) zigzag (Z) configurations. The isosurface for all structures corresponds to charge densities with the isovalue of 0.025 $e/Å^3$.

Table 1
The parameters E_b and q represent the calculated amount of binding energy and charge transfer between Li and graphane after atomic relaxation, respectively. d_{Li-C} (Å) is the relaxed bond distance between Li and C, and Δd_{Li-C} is the difference between the relaxed and initial bond distance (2.10 Å optimum distance for Li on graphene).

Li sites	E_b (eV)	q (e)	d_{Li-C} (Å)	Δd_{Li-C}
		Li on pristine graphane		
Li–H	−1.73	0.30	3.78	1.69
Li–C	−0.22	0.28	3.68	1.58
Li–B	−0.22	0.28	3.67	1.57
Li–h	−0.22	0.28	3.76	1.66
Li–graphene	1.10[a], 1.29[b]	0.90[a]	1.71[a], 1.71[b]	
		Li on graphane with V_H		
Li–V_H	1.82	0.90	2.07	−0.03
Li–C′	1.85	0.88	2.01	−0.09
Li–b′	1.85	0.89	2.02	−0.08
Li–h′	1.82	0.90	2.04	−0.06

[a] Ref [21].
[b] Ref [45].

For the zigzag (Z) configuration, the localized electrons on the nearest neighbour C atoms (V_{H1}(Z)) and V_{H2}(Z) as shown in Fig. 2(c) pair and form the π bonding network. This bonding re-constructions could be responsible for less formation energy in zigzag (Z), as compared to other configurations. For the line (L) and random (R) configurations, there will be no possibilities of localized electron pairing as shown in structural arrangement in Figs. 2 (a) and (b), and this could be the reason for the relative high formation energies. Based on the stability findings, the Li adatoms will be adsorbed on zigzag (Z) and Line (L) configuration. These configurations (zigzag (Z) and Line (L)) will easily allow Li adatoms to be channelled without interfering with H atoms unlike in random vacancies were each V_H is surrounded by H atoms.

To get insight on the effect of these V_H configurations on the nature of bonding of graphane, the charge densities are presented in Fig. 4. For a pristine graphane monolayer, at the isovalue of 0.025 $e/Å^3$ (utilizing VESTA software [44]), the charges are uniformly distributed and concentrated around each carbon preserving sp^3 hybridized bonding network. Both the zigzag (Z) and Line (L) configurations alter the charge density distribution of pristine graphane. The carbon atom with the V_H has a dangling bond (localized electron) turning into sp^2 hybridized bonding network, thereby increasing the cloud of charge at the vicinity of the vacancy. Increasing the vacancies following a periodic pattern along the zigzag (Z) and Line (L) configurations could lead to increase in the dangling bonds that manifest a pronounced cloud of charge character along one dimension as shown in Figs. 4(b) and (c).

The binding energies (E_b), which is defined as the amount of energy required to remove the adatoms from the graphane sheet for the interaction to be minimal, can be used to determine how Li adatoms bound with the graphane sheet. Importantly, the E_b will guide on the charge storage capacity, more especially when the Li concentration increases. In this study, the binding energies between Li and the following sites: b_{site}, h_{site}, H_{site}, C_{site}, b'_{site}, h'_{site}, $V_{H\,site}$ and C'_{site}, were calculated using Eq. (5) below, to find the most energetically favourable adsorption site:

$$E_b = \frac{E(CHLi) - E(CH) - nE(Li)}{n} \tag{3}$$

where $E(CHLi)$, $E(CH)$ and $E(Li)$ in Eq. (5) represent the relaxed total energies of Li adsorbed on graphane structure, graphane structure and isolated Li atom obtained from a converged large cubic box of lattice constants of 10 Å. The n represents number of Li atoms adsorbed. The values of the calculated E_b are shown in Table 1. As opposed to the interpretation of the well known adsorption energy of the adsorbent, the positive value of the binding energy suggests the possibility of great interaction (energetically favourable) whereas the negative value means minimal interaction (not energetically favourable). The Li b_{site}, h_{site}, H_{site} and C_{site} configurations have negative binding energies, indicating that they are energetically not favourable. Therefore, Li atoms do not bind with graphane monolayer. This is supported by the relatively large d_{Li-C} of 3.78 Å (H_{site}), 3.68 Å (C_{site}), 3.67 Å (b_{site}) and 3.76 Å (h_{site}) compared to the 2.10 Å value of Li on graphene. Experimental study by Watcharinyanon et al. [31] reports that Li atoms form islands above the graphane, and disappear during annealing. The positive Δd_{Li-C} suggests the possibility of ionic repulsion between Li and H atoms from the initial bond distance of 2.10 Å. These results are in agreement with the observation of Yang et al. [30].

To further quantify an interaction between Li and pristine graphane, Li charge transfer (q) was calculated using the Bader analysis method [46] implemented in the Vasp. The positive value of q suggests the possibility of an atom to give a charge whereas negative value implies an atom accepts a cloud of charge. The charge transfer for Li on four different sites (b_{site}, h_{site}, H_{site} and C_{site}) was found to averagely be 0.28e. This value is far smaller than that of Li on graphene of 0.90e [21]. The remaining electronic charge of 0.72e on Li is enough to form a strong covalent bond with other Li atoms which could possibly lead to unwanted Li-ion clustering. The partial charge transfer analysis reveals that 0.28e amount of charge is mainly accepted by an H atom facing the Li adatom. This is in agreement with Yang et al. [30] who reported that the Li ionic charges are screened by H atoms on graphane. These preliminary results indicate that it is unlikely for the Li adatoms to be uniformly distributed above the graphane monolayer, hence support an idea that it will not be suitable for hosting Li atoms for LIBs.

To investigate the possibility of improving interaction of Li with graphane for LIBs, a V_H was created. In this situation, Li atom is adsorbed on the four distinct sites namely: b'_{site}, h'_{site}, $V_{H\,site}$ and C'_{site} depicted in Fig. 1(b). The corresponding E_b and d_{Li-C} are presented in Table 1. The calculated E_b for b'_{site}, h'_{site}, $V_{H\,site}$ and C'_{site} are positive, suggesting an enhanced interaction between Li and graphane. The above results are in agreement with the work of Hussain et al. [37]. The E_b values for the $V_{H\,site}$, C'_{site}, b'_{site} and h'_{site} configurations are 1.82 eV, 1.85 eV, 1.85 eV and 1.82 eV, respectively. The E_b values for these Li configurations are very close, however, they only differ in the second decimal place. This could be due to the consequence of the same nearest neighbour C atoms as well as the same coordination number for all sites as shown in Fig. 5. These binding energy values are more than

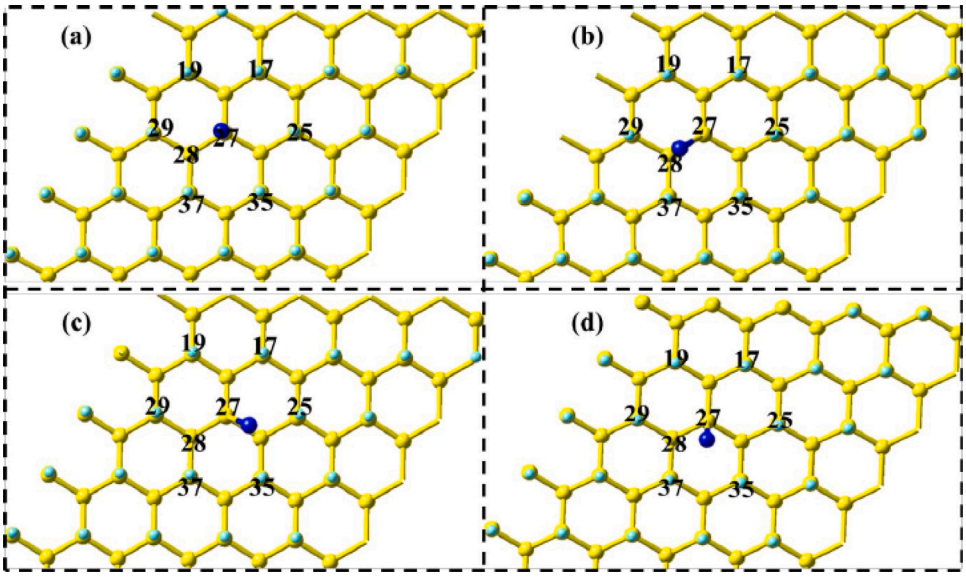

Fig. 5. The relaxed structures of different Li configurations on graphane(a) $V_{H\,site}$, (b) C'_{site}, (c) b'_{site} and (d) h'_{site}. The numbered atoms are those significantly affected by Li adsorption.

the calculated bulk cohesive energy (1.48 eV) of Li in a body centred cube (BCC) structure. The theoretical value of the bulk cohesive energy is reported to be 1.63 eV. Our results suggest the possibility of having a uniform dispersion of Li atoms with less clustering on the graphane sheet.

From the Li initial position of 2.10 Å above the graphane sheet, Li atom tends to relax towards the sheet, hence the negative values of Δd_{Li-C} shown in Table 1. The above scenario suggests a possible induced Li-ions interacting with localized dangling electronic bonds at the $V_{H site}$. The calculated d_{Li-C} for all sites as shown in Table 1 are in good agreement with the results in Refs. [36,37]. When Li is on top of the $V_{H site}$ vacancy, the d_{Li-C} is 2.07 Å. However, that of the h'_{site}, and C'_{site} are 2.02 Å and 2.01 Å, respectively. Due to atomic position relaxations, Li atom shifts from its initial position of C'_{site}, b'_{site} and h'_{site} towards the $V_{H site}$, as shown in Fig. 5. For instance, in the case of h'_{site} the Li shifts from the centre of hexagon and relaxes towards the H vacancy as shown in Fig. 5(d). This is in contrast to the case of graphene where Li atom is stable at the centre of hexagon [45]. For $V_{H site}$, the Li atom remains on top after atomic relaxation.

As shown in Table 1, the creation of V_H vacancy on graphane has a significant increase on the Coulomb interactions between Li atom and graphane, as enhanced amount of charge transfer is noted. All the four Li atom configurations uniformly transfer almost up to 90% of the charge to the substrate. As an indication of induced ionic (Li) and localized electronic (C connecting V_H) interactions. We further performed partial charge transfer analysis calculations to identify the host atoms that are likely to receive a great amount of Li charge. The numbered atoms to likely receive the Li charge are depicted in Fig. 5. The amount of Li charge transferred is shared by C27 (V_H) and its surrounding H atoms (H17, H19, H25, H26, H35 and H37). In all the Li configurations considered, the C27 receives a fraction of 0.43e while the surrounding H atoms each receives an electron charge of 0.09e on the average indicating the possibility of charge shielding by H atoms.

From the information above it is clear that creation of the H vacancies mediate interaction of Li with graphane. We further examined influence of the multiple V_H vacancies and Li atoms on the enhanced energetic stability, voltage potential and storage capacity. We systematically increased the number of H vacancies (V_H) as well as the Li content along the extended pathways as shown in Fig. 2 (each Li atom is adsorbed on top of a V_H vacancy). Fig. 6(a) presents the calculated binding energies with respect to the number of Li atoms occupying the V_H vacancies along the line as well as along the zigzag pathways. Simultaneous increase of Li content and V_H leads to a decrease in the binding energy, suggesting the possibility of Li–Li interactions, in agreement with the previous study for other graphene related materials [47].

For the zigzag pathway, the increment of Li atoms reduces the binding energy substantially as shown in Fig. 6(a). For instance, when the second Li atom is added to form the $V_{H2(Z)}$ configuration, the binding energy reduces from 1.82 eV to 0.80 eV. This is due to the pairing of the electrons from the nearest neighbour C atoms ($V_{H1(Z)}$ and $V_{H2(Z)}$), which seems to repel the Li atoms, giving rise to high energy configuration $V_{H2(Z)}$. The small amount of charge transfer of 0.5e supports poor Li–$V_{H2(Z)}$ interaction shown in Fig. 6(b). For $V_{H3(Z)}$, the binding energy increases to 1.04 eV. This could be attributed to the availability of the unpaired electron, consequent of the third V_H accepting the Li charge of 0.72e. Although, the binding energy rises, is below that of the required Li standard bulk cohesive energy of 1.63 eV. The poor binding occurs for $V_{H2(Z)}$ even up to the $V_{H10(Z)}$ configuration with an average binding energy of 0.93 eV. This value suggests that the Li atoms will resort to cluster formation which will probably lead to undesired dendrite substances formation.

The $V_{H1(L)}$, $V_{H2(L)}$, $V_{H3(L)}$ and $V_{H5(L)}$ configurations have binding energies of 1.82 eV, 1.68 eV, 1.78 eV and 1.48 eV, respectively, as shown in Fig. 6(a). The relative small binding energy differences shown in Fig. 6(a) suggests that more Li atoms are needed before Li clusters formation. These binding energy values are comparable to the required Li standard bulk cohesive energy of 1.63 eV. Fig. 6(b) shows a slight decrease in the charge transfer as the number of Li atoms increases. The lowest charge transfer (0.80e) is observed in the case of $V_{H5(L)}$ configuration. Since the V_H vacancies along the line consistently give the high binding energies and charge transfer, we adopt this pathway for electronic and electrochemical properties calculations.

3.1. Electronic and electrochemical properties of Li on graphane with V_H along the line pathway

We further investigate the effect of multiple H vacancies and Li atoms ($V_{H1(L)}$, $V_{H2(L)}$, $V_{H3(L)}$, $V_{H4(L)}$ and $V_{H5(L)}$) on the electronic properties of graphane. The density of states (DOS) plot for the pristine graphane is presented in Fig. 7(a). It is shown that pristine graphane possesses a wide energy band gap of 3.70 eV between the valence band maximum (VBM) and conduction band minimum (CBM), exhibiting an insulating material, agreeing very well with the previous studies [28,

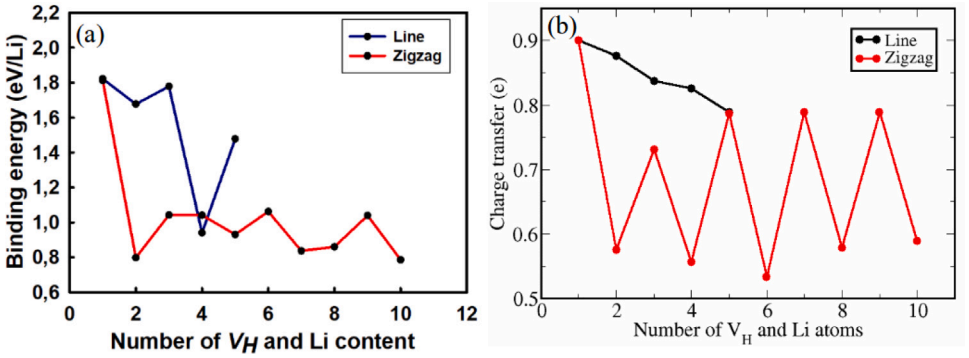

Fig. 6. (a) The calculated binding energies for multiple Li atoms adsorbed on the V_H vacancies along the line as well as along the zigzag pathways. (b) The amount of charge transfer obtained from the Bader analysis on the multiple Li atoms adsorbed on the V_H vacancies.

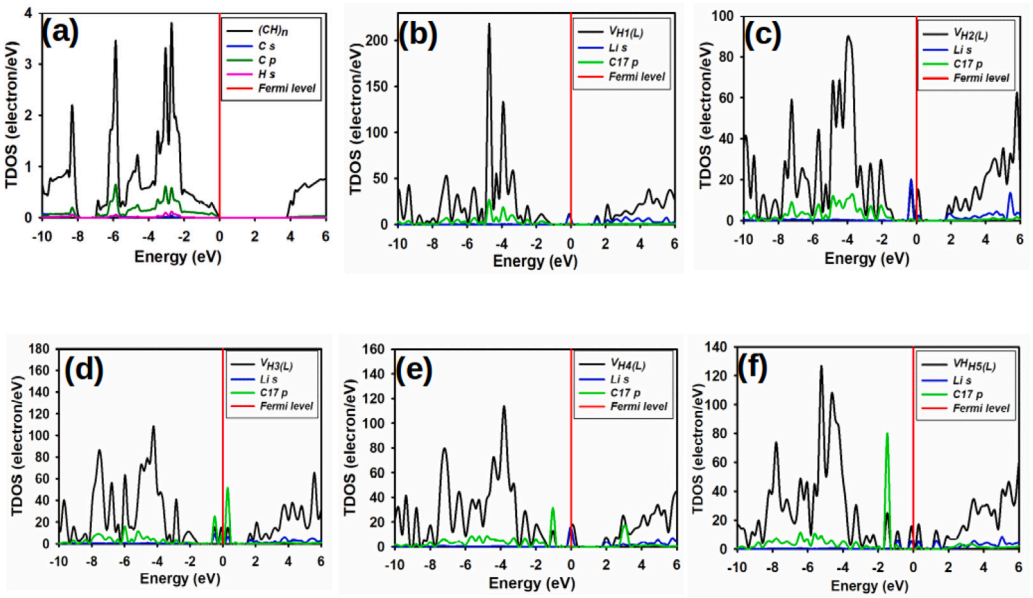

Fig. 7. (a) The total density of states (TDOS) and partial density of states (PDOS) of a (a) pristine graphane (CH) monolayer. DOS of variable Li atoms and number of V_H along the Line path (b) $V_{H1(L)}$, (c) $V_{H2(L)}$, (d) $V_{H3(L)}$, (e) $V_{H4(L)}$ and (f) $V_{H5(L)}$. The Fermi level is set at 0.00 eV and represented by the red line.

34]. Both the VBM and CBM are mainly contributed by the *p* orbital states. The wide band gap characteristic suggests a poor electrical conductivity that will possibly limit the electronic transmission in the graphane during LIBs operation. Figs. 7(b)–(f) show the DOS plots of the $V_{H1(L)}$, $V_{H2(L)}$, $V_{H3(L)}$, $V_{H4(L)}$ and $V_{H5(L)}$, respectively.

It is observed that the adsorption of Li on $V_{H1(L)}$, $V_{H2(L)}$, $V_{H3(L)}$, $V_{H4(L)}$ and $V_{H5(L)}$ introduces new electronic states at the vicinity of the Fermi level, and also shifting the Fermi level to the conduction band minimum (CBM). This is due to an excess of electrons donated by Li (*s* orbital states) adatoms and the existence of electron dangling bonds (*p* orbital) at the V_H in the systems. The electronic peaks at the Fermi level rises with the concentration as shown in Figs. 7(b)–(f), suggesting that a Coulomb interactions become more stronger between Li ions on the graphane system. Fig. 7(f) shows that the simultaneous increase of vacancies and Li adatoms by a small concentration of 0.1, fill the entire band gap with the induced electronic states. Hence, the improved metallic character in this configurations is expected to enhance electrical conductivity leading to a great electron transmission performance in the graphane.

For graphane to be applied as an electrode in LIB, it must have a high storage capacity. The Li storage capacities of $V_{H1(L)}$, $V_{H2(L)}$, $V_{H3(L)}$ and $V_{H5(L)}$ configurations were calculated and compared with other two dimensional anode materials. The storage capacities were calculated using the following expression [48], and the results were plotted as shown in Fig. 8(a). The storage capacity as a function of number of Li atoms is given as:

$$C = \frac{nF}{M} \times \frac{1000}{3600}, \tag{4}$$

where n represents the number of Li-ions adsorbed on graphane, F is the Faraday's constant (F = 96 500 C/mol) and M is the molar mass of graphane. The Coulomb to mAh conversion factor is 1000/3600. For $V_{H1(L)}$, $V_{H2(L)}$, $V_{H3(L)}$ and $V_{H5(L)}$, the relatively high storage capacity of 207.49 mAh/g was obtained as shown in Fig. 8(a). This value is comparable to those of Li at high concentration on other anode materials such as MoS_2 (146 mAh/g) [49] and $Li_{6.84}B_2C_{70}$ (212.6 mAh/g) [50]. It is anticipated that at maximum concentration of Li on graphane, the storage capacity will be more than that of standard graphite (372 mAh/g).

Another way to gain better understanding of the performance of Li adsorbed graphane as a suitable anode material for LIBs is by calculating the lithiation potential (υ). It is well known that a small theoretical υ in an electrode hinders the formation of unwanted dendrites but keeping the energy density high [51], which suitable is for LIBs. The υ is calculated using the following equation [48] and plotted as a function of number of Li atoms in Fig. 8(b):

$$\upsilon = -\frac{E(LiCH) - E(CH) - nE(Li)}{nzF}. \tag{5}$$

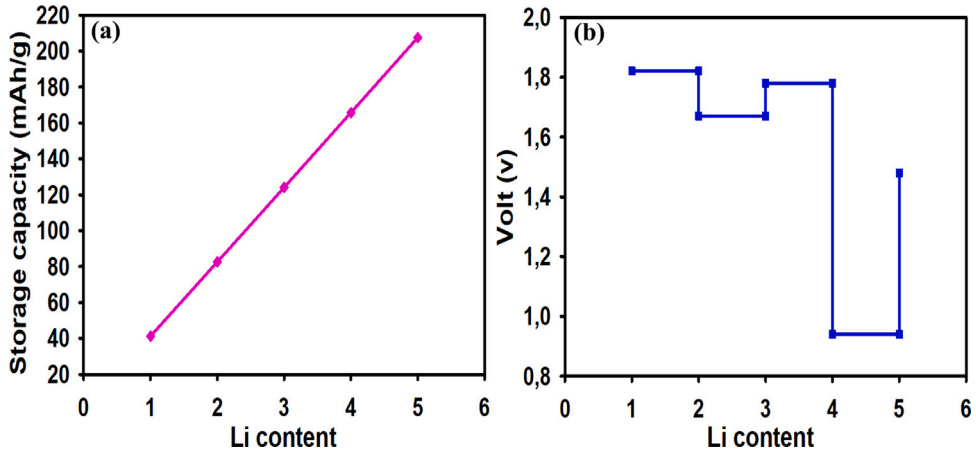

Fig. 8. (a) The Li storage capacity with respect to the increase in Li content. (b) Lithiation potential (voltage) with respect to the increase in Li content. Configurations considered are $V_{H1(L)}$, $V_{H2(L)}$, $V_{H3(L)}$ and $V_{H5(L)}$.

In Eq. (5), the z is the electronic charge of Li ions in the electrolyte (in this case z = 1). It is noteworthy to know that the positive value of υ will ensures that the adsorption of Li on graphane anode material will be possible without clustering formation. The calculated υ for the $V_{H1(L)}$, $V_{H2(L)}$, $V_{H3(L)}$, $V_{H4(L)}$ and $V_{H5(L)}$ ranges from 1.8 V–0.92 V. The υ fluctuation as the number of Li atoms increases (see Fig. 8(b)) is an indication that this property depends on the number of adatoms as well as the structural reconstruction of the atoms during relaxation. Due to υ taking the form of E_b which depends on the compound structural properties. The value of υ will only approach zero when the Li atoms reaches maximum adsorption. For $V_{H1(L)}$, $V_{H2(L)}$, $V_{H3(L)}$, $V_{H4(L)}$ and $V_{H5(L)}$, the average υ is 1.51 V. This is an indication that more Li adatoms are still needed before the required range of 0 V–1 V [51] can be reached. The results suggest that the formation of lithium dendrites during the charge and discharge cycles will not be easy. The values of υ for $V_{H1(L)}$, $V_{H2(L)}$, $V_{H3(L)}$, $V_{H4(L)}$ and $V_{H5(L)}$ within the range of 1.8 V to 0.92 V are comparable to those of Li on B doped graphene [50] and Be doped graphene [48].

4. Conclusions

Enhancement of Li–graphane interaction for selected properties of LIBs has been successfully investigated using DFT calculations. To improve the Li–graphane interactions, multiple H vacancies (V_H) were designed to induce dangling bonds for the line and zigzag pathways configurations on a 5 × 5 × 1 graphane supercell. The results of Li on a single H vacancy V_{H1} revealed an improved interaction due to the improved binding energies, charge transfer and significantly shortened Li height as compared to the pristine graphane.

The adsorption of Li atoms along the line pathway is more energetically favourable than those along the zigzag pathway. The localized electrons around the vacancies in zigzag configuration pair, and repel the Li ions, while in the line configuration there is no possibility of electronic pairing, leading to Li ions strongly interacting with vacancies. For increment of Li content following a line $V_{H(L)}$ pathway, the binding energies of Li on configurations $V_{H1(L)}$ to $V_{H5(L)}$ tend to slightly reduce, due to the possibility of Li–Li interaction. These Li configurations have metallic character and their conductivity increase with Li content due to more states been populated in the band gap which will enhance the electron transmission in a graphane sheet. At five Li content adsorbed along line configurations, a relatively high storage capacity of 207.49 mAh/g with its corresponding lithiation potential of 1.48 V are achieved and are comparable to the other previously studied 2D anode materials with high Li concentration. The efficiency of our obtained results suggests that graphane sheet with far distant H vacancies can be a promising 2D anode material for LIBs.

CRediT authorship contribution statement

S.P. Kgalema: Conceived and designed the analysis, Analyzed and interpreted the data, Contributed analysis tools, Writing – original draft. **M. Diale:** Conceived and designed the analysis, Analyzed and interpreted the data, Contributed analysis tools, Writing – original draft. **E. Igumbor:** Conceived and designed the analysis, Analyzed and interpreted the data, Contributed analysis tools, Writing – original draft. **R.E. Mapasha:** Conceived and designed the analysis, Analyzed and interpreted the data, Contributed analysis tools, Writing – original draft.

Declaration of competing interest

The authors declare that they have no known competing financial interests or personal relationships that could have appeared to influence the work reported in this paper.

Data availability

Data will be made available on request.

Acknowledgements

Authors would like to thank the University of Pretoria for financial support and availability of the state-of-the-art computational resources. SPK and REM acknowledge financial support from the NITheCS program, South Africa. REM is also grateful to NRF, South Africa for financial support. Profs W. Meyer and J. Pretorius are acknowledged for Medea VASP technical support. Authors also thanks Center for high performance computing in cape town for state-of-the-art resources.

References

[1] D. Ibrahim, Renewable energy and sustainable development: A crucial review, Renew. Sustain. Energy Rev. 4 (2000) 157–175, http://dx.doi.org/10.1016/S1364-0321(99)00011-8.

[2] K. Alyssa, G. Karl, Promoting geothermal energy: Air emissions comparison and externality analysis, Electr. J. 18 (2005) 90–99, http://dx.doi.org/10.1016/j.tej.2005.07.004.

[3] D. Kaoshan, B. Anthony, L.C. Xiang, W. Ning, H. Zhenhua, Environmental issues associated with wind energy – A review, Renew. Energy 75 (2015) 911–921, http://dx.doi.org/10.1016/j.renene.2014.10.074.

[4] J.A. Turner, A realizable renewable energy future, Science 285 (1999) 687–689, http://dx.doi.org/10.1126/science.285.5428.687.

[5] B. Scrosati, J. Hassoun, Y.-K. Sun, Lithium-ion batteries. A look into the future, Energy Environ. Sci. 4 (2011) 3287–3295, http://dx.doi.org/10.1039/C1EE01388B.

[6] D. Deng, Li-ion batteries: basics, progress, and challenges, Energy Sci. Eng. 3 (2015) 385–418, http://dx.doi.org/10.1002/ese3.95.

[7] A.G. Pandolfo, A.F. Hollenkamp, Carbon properties and their role in supercapacitors, J. Power Sources (ISSN: 0378-7753) 157 (1) (2006) 11–27, http://dx.doi.org/10.1016/j.jpowsour.2006.02.065.

[8] P. Siwatch, K. Sharma, A. Arora, S.K. Tripathi, Review of supercapacitors: Materials and devices, J. Energy Storage 21 (2019) 801–825, http://dx.doi.org/10.1016/j.est.2019.01.010.

[9] George Blomgren, The development and future of lithium ion batteries, J. Electrochem. Soc. 164 (2017) A5019–A5025, http://dx.doi.org/10.1149/2.0251701jes.

[10] Bingkun Guo, Xiqing Wang, Pasquale Fulvio, Miaofang Chi, Shannon Mahurin, Xiao-Guang Sun, Sheng Dai, Soft-templated mesoporous carbon-carbon nanotube composites for high performance lithium-ion batteries, Adv. Mater. (Deerfield Beach, Fla.) 23 (2011) 4661–4666, http://dx.doi.org/10.1002/adma.201102032.

[11] J.R. Dahn, Tao Zheng, Yinghu Liu, J.S. Xue, Mechanisms for lithium insertion in carbonaceous materials, Science 270 (5236) (1995) 590–593, http://dx.doi.org/10.1126/science.270.5236.590.

[12] P. Simon, Y. Gogotsi, B. Dunn, Where do batteries end and supercapacitors begin? Science 343 (2014) 1210–1211, http://dx.doi.org/10.1126/science.1249625.

[13] Guangli Che, Brinda B. Lakshmi, Ellen R. Fisher, Charles R. Martin, Carbon nanotubule membranes for electrochemical energy storage and production, Nature 393 (6683) (1998) 346–349, http://dx.doi.org/10.1038/30694, URL https://ideas.repec.org/a/nat/nature/v393y1998i6683d10.1038_30694.html.

[14] K.S. Novoselov, A.K. Geim, S.V. Morozov, D. Jiang, Y. Zhang, S.V. Dubonos, I.V. Grigorieva, A.A. Firsov, Electric field effect in atomically thin carbon films, Science 306 (2004) 666.

[15] A.K. Geim, K.S. Novoselov, The rise of graphene, Nature Mater. 6 (2007) 183–191.

[16] A.A. Balandin, S. Ghosh, W. Bao, I. Calizo, D. Teweldebrhan, F. Miao, C.N. Lau, Superior thermal conductivity of single–layer graphene, Nano Lett. 8 (2008) 902–907.

[17] K.S. Novoselov, V.I. Falko, L. Colombo, P.R. Gellert, M.G. Schwab, A.K. Kim, A roadmap for graphene, Nature 490 (2012) 192–200.

[18] Daniel Cunha Elias, Reghunadhan Nair, Tariq Mohiuddin, S. Morozov, P. Blake, M. Halsall, A.C. Ferrari, D. Boukhvalov, Mikhail Katsnelson, A.K. Geim, K. Novoselov, Control of graphene's properties by reversible hydrogenation: Evidence for graphane, Science 323 (2009) 610–613, http://dx.doi.org/10.1126/science.1167130.

[19] M.D. Stoller, S. Park, Y. Zhu, J. An, R.S. Ruoff, Graphene-based ultracapacitors, Nano Lett. 8 (2008) 3498–3502.

[20] M. Xu, T. Liang, M. Shi, H. Chen, Graphene-based ultracapacitors, Chem. Rev. 113 (2013) 3766–3798.

[21] Kevin T. Chan, J.B. Neaton, Marvin L. Cohen, First-principles study of metal adatom adsorption on graphene, Phys. Rev. B 77 (2008) 235430, http://dx.doi.org/10.1103/PhysRevB.77.235430, URL https://link.aps.org/doi/10.1103/PhysRevB.77.235430.

[22] Xiaofeng Fan, W.T. Zheng, Jer-Lai Kuo, Adsorption and diffusion of Li on pristine and defective graphene, ACS Appl. Mater. Interfaces 4 (5) (2012) 2432–2438, http://dx.doi.org/10.1021/am3000962, PMID: 22536839.

[23] Xiaofeng Fan, W.T. Zheng, Jer-Lai Kuo, David J. Singh, Adsorption of single Li and the formation of small Li clusters on graphene for the anode of lithium-ion batteries, ACS Appl. Mater. Interfaces 5 (16) (2013) 7793–7797, http://dx.doi.org/10.1021/am401548c, PMID: 23863039.

[24] Yuanyue Liu, Vasilii I. Artyukhov, Mingjie Liu, Avetik R. Harutyunyan, Boris I. Yakobson, Feasibility of lithium storage on graphene and its derivatives, J. Phys. Chem. Lett. 4 (10) (2013) 1737–1742, http://dx.doi.org/10.1021/jz400491b, PMID: 26282987.

[25] J. Song, B. Ouyang, N.V. Medhekar, Energetics and kinetics of Li intercalation in irradiated graphene scaffolds, ACS Appl. Mater. Interfaces 5 (24) (2013) 12968–12974, http://dx.doi.org/10.1021/am403685w, PMID: 24256350.

[26] Eunseok Lee, Kristin A. Persson, Li absorption and intercalation in single layer graphene and few layer graphene by first principles, Nano Lett. 12 (9) (2012) 4624–4628, http://dx.doi.org/10.1021/nl3019164, PMID: 22920219.

[27] Marcel H.F. Sluiter, Yoshiyuki Kawazoe, Cluster expansion method for adsorption: Application to hydrogen chemisorption on graphene, Phys. Rev. B 68 (2003) 085410, http://dx.doi.org/10.1103/PhysRevB.68.085410, URL https://link.aps.org/doi/10.1103/PhysRevB.68.085410.

[28] Jorge O. Sofo, Ajay S. Chaudhari, Greg D. Barber, Graphane: A two-dimensional hydrocarbon, Phys. Rev. B 75 (2007) 153401, http://dx.doi.org/10.1103/PhysRevB.75.153401, URL https://link.aps.org/doi/10.1103/PhysRevB.75.153401.

[29] H. Sahin, O. Leenaerts, S.K. Singh, F.M. Peeters, Graphane, WIREs Comput. Mol. Sci. 5 (3) (2015) 255–272, http://dx.doi.org/10.1002/wcms.1216, URL https://wires.onlinelibrary.wiley.com/doi/abs/10.1002/wcms.1216.

[30] Y.E. Yang, Y. Xiao, X.H. Yan, Charge distribution of lithium-doped graphane/graphene hybrid system: Role of nearly-free electronic states, Solid State Commun. (ISSN: 0038-1098) 229 (2016) 43–48, http://dx.doi.org/10.1016/j.ssc.2015.12.011, URL https://www.sciencedirect.com/science/article/pii/S0038109815004366.

[31] S. Watcharinyanon, C. Virojanadara, Jacek Osiecki, A. Zakharov, Rositsa Yakimova, R. Uhrberg, Leif Johansson, Hydrogen intercalation of graphene grown on 6H-SiC(0001), Surf. Sci. 605 (2011) 1662–1668, http://dx.doi.org/10.1016/j.susc.2010.12.018.

[32] Bhalchandra S. Pujari, D.G. Kanhere, Density functional investigations of defect-induced mid-gap states in graphane, J. Phys. Chem. C 113 (50) (2009) 21063–21067, http://dx.doi.org/10.1021/jp907640t.

[33] R.E. Mapasha, M.P. Molepo, N. Chetty, Ab initio studies of isolated hydrogen vacancies in graphane, Physica E (ISSN: 1386-9477) 79 (2016) 52–58, http://dx.doi.org/10.1016/j.physe.2015.12.014, URL https://www.sciencedirect.com/science/article/pii/S1386947715303246.

[34] R.E. Mapasha, M.P. Molepo, N. Chetty, Li states on a C–H vacancy in graphane: a first-principles study, RSC Adv. 7 (2017) 39748–39757, http://dx.doi.org/10.1039/C7RA06431D.

[35] J. Kotakoski, A.V. Krasheninnikov, U. Kaiser, J.C. Meyer, From point defects in graphene to two-dimensional amorphous carbon, Phys. Rev. Lett. 106 (2011) 105505, http://dx.doi.org/10.1103/PhysRevLett.106.105505, URL https://link.aps.org/doi/10.1103/PhysRevLett.106.105505.

[36] Tanveer Hussain, Biswarup Pathak, Tuhina Adit Maark, Carlos Moyses Araujo, Ralph H. Scheicher, Rajeev Ahuja, Ab initio study of lithium-doped graphane for hydrogen storage, Europhys. Lett. 96 (2) (2011) 27013, http://dx.doi.org/10.1209/0295-5075/96/27013.

[37] Tanveer Hussain, Abir De Sarkar, Rajeev Ahuja, Strain induced lithium functionalized graphane as a high capacity hydrogen storage material, Appl. Phys. Lett. 101 (10) (2012) 103907, http://dx.doi.org/10.1063/1.4751249.

[38] Pierre Hohenberg, Walter Kohn, Inhomogeneous electron gas, Phys. Rev. 136 (3B) (1964) B864.

[39] W. Kohn, L.J. Sham, Self-consistent equations including exchange and correlation effects, Phys. Rev. 140 (1965) A1133–A1138, http://dx.doi.org/10.1103/PhysRev.140.A1133, URL https://link.aps.org/doi/10.1103/PhysRev.140.A1133.

[40] Peter Blöchl, Clemens Först, Johannes Schimpl, Projector augmented wave method: Ab initio molecular dynamics with full wave functions, Bull. Mater. Sci. 26 (2003) 33–41, http://dx.doi.org/10.1007/BF02712785.

[41] G. Kresse, J. Hafner, Ab initio molecular dynamics for liquid metals, Phys. Rev. B 47 (1993) 558–561, http://dx.doi.org/10.1103/PhysRevB.47.558, URL https://link.aps.org/doi/10.1103/PhysRevB.47.558.

[42] John P. Perdew, Kieron Burke, Matthias Ernzerhof, Generalized gradient approximation made simple, Phys. Rev. Lett. 77 (1996) 3865–3868, http://dx.doi.org/10.1103/PhysRevLett.77.3865, URL https://link.aps.org/doi/10.1103/PhysRevLett.77.3865.

[43] Hendrik J. Monkhorst, James D. Pack, Special points for Brillouin-zone integrations, Phys. Rev. B 13 (1976) 5188–5192, http://dx.doi.org/10.1103/PhysRevB.13.5188, URL https://link.aps.org/doi/10.1103/PhysRevB.13.5188.

[44] K. Momma, F. Izumi, VESTA 3 for three-dimensional visualization of crystal, volumetric and morphology data, J. Appl. Crystallogr. 44 (2011) 1272–1276.

[45] A.M. Garay-Tapia, Aldo H. Romero, Veronica Barone, Lithium adsorption on graphene: From isolated adatoms to metallic sheets, J. Chem. Theory Comput. 8 (3) (2012) 1064–1071, http://dx.doi.org/10.1021/ct300042p, PMID: 26593367.

[46] List of publications for Richard F. W. Bader, J. Phys. Chem. A 115 (45) (2011) 12438–12444, http://dx.doi.org/10.1021/jp208984n, PMID: 22070782.

[47] Sankha Mukherjee, Avinav Banwait, Sean Grixti, Nikhil Koratkar, Chandra Veer Singh, Adsorption and diffusion of lithium and sodium on defective rhenium disulfide: A first principles study, ACS Appl. Mater. Interfaces 10 (6) (2018) 5373–5384, http://dx.doi.org/10.1021/acsami.7b13604, PMID: 29350901.

[48] Saif Ullah, Pablo A. Denis, Fernando Sato, Beryllium doped graphene as an efficient anode material for lithium-ion batteries with significantly huge capacity: A DFT study, Appl. Mater. Today 9 (2017) 333–340.

[49] Majid Mortazavi, Chao Wang, Junkai Deng, Vivek Shenoy, Nikhil Medhekar, Ab initio characterization of layered MoS2 as anode for sodium-ion batteries, J. Power Sources 268 (2014) 279–286, http://dx.doi.org/10.1016/j.jpowsour.2014.06.049.

[50] Liujiang Zhou, Z.F. Hou, Bo Gao, Thomas Frauenheim, Doped graphenes as anodes with large capacity for lithium-ion batteries, J. Mater. Chem. A 4 (2016) 13407–13413, http://dx.doi.org/10.1039/C6TA04350J.

[51] L. Shi, T.S. Zhao, A. Xu, J.B. Xu, Ab initio prediction of a silicene and graphene heterostructure as an anode material for Li- and Na-ion batteries, J. Mater. Chem. A 4 (2016) 16377–16382, http://dx.doi.org/10.1039/C6TA06976B.